Supporting Materials

Low tortuous, highly conductive, and high-areal-capacity battery electrodes enabled by through-thickness aligned carbon fiber framework

Baohui Shi[1,‡], Yuanyuan Shang[1,‡], Yong Pei[2], Shaopeng Pei[1], Liyun Wang[1], Dirk Heider[3,5], Yong (Y.) Zhao[4], Chaolun Zheng[2], Bao Yang[2], Shridhar Yarlagadda[3,5,*], Tsu-Wei Chou[1,3], Kun (Kelvin) Fu[1,3,*]

[1]Department of Mechanical Engineering, University of Delaware, Newark, DE 19716, USA
[2]Department of Mechanical Engineering, University of Maryland, College Park, MD 20742, USA
[3]Center for Composite Materials, University of Delaware, Newark, DE 19716, USA
[4]Department of Materials Science & Engineering, University of Delaware, Newark, DE 19716, USA
[5]Electrical & Computer Engineering, University of Delaware, Newark, DE 19716, USA

‡ These authors contributed equally to this work.

* Corresponding authors

Emails: kfu@udel.edu, yarlagad@udel.edu

Experimental Section

Thick electrode fabrication

Fiber-aligned membrane: The membrane was made of IM7 carbon fibers. The carbon fibers are cut into short fibers with a length of 3mm and a diameter of 5 μm.

Aqueous electrode ink: Commercial $LiFePO_4$ (LFP) nanoparticles (MTI), carbon black (CB) and sodium carboxymethylcellulose (CMC) binder were mixed together in water with a weight ratio of 9:0.5:0.5 to make the slurry. The mixed solution was magnetic stirred for 100 h to obtain the uniformly dispersed LFP nanoparticles solution.

Electrode material-loaded membrane: The mixed solution (LFP, CMC and water) was coated onto fiber-aligned membrane by a roller. After coating, the composite membrane was dried under the vacuum at 60°C for 24 h and then at 80°C for 24 h to evaporate the solvent. After drying, the composite membrane was rolled up into a cylindrical shape rod. The weight ratio of LFP, carbon fiber (CF) and carbon black, and CMC binder is 73%, 25% and 2%. The rod was then cut in the radial direction to obtain the fiber-aligned thick electrode.

$LiFePO_4$ (LFP) nanoparticles (MTI), carbon black (CB) and sodium carboxymethylcellulose (CMC) binder were mixed together by mixer for 1 hour. Water is the solvent and the LFP, CB, and CMC ratio is 7.4:2.4:0.2. The slurry was then coated by doctor blade on an Al foil dried at 80 ºC for 12 hours. To achieve high LFP mass loading, the coating process was repeated several times through layer-by-layer coating. The final electrode was then vacuum dried at 80°C for 24 hours before transferring into Ar-filled glovebox.

Characterizations

The morphologies of electrodes materials were characterized by scanning electron microscopy (SEM, SEM/FIB Auriga 60 CrossBeam). Electronic conductivity of the FAT electrode and slurry-

electrodes was measured by the Keithley 2425 SourceMeter using a four-point probe method. The Micro-CT (SkyScan 1172 Micro CT) conducted on CCM (Newark, Delaware, USA) provided 3D images on the FAT electrode architecture. The surface temperature of the electrodes was measured by an infrared camera (FLIR ETS320). The temperature was recorded using the software of FLIR Tools+.

Mechanical compression test

The compressive strengths of the FAT electrode and slurry-casted thick electrodes were evaluated using Instron 5848 machine. A strain rate of 0.25 mm/min was applied to electrode samples. Modulus was obtained from the initial slope of the stress–strain curve over a strain range of 0.2%-0.4%. The maximum strength is defined as the maximum value of stress-strain curve before serious failure occurs. The failure is caused by the tilt of aligned carbon fibers under high compression. The FAT electrode after compression test retained electrode shape with minor tilting in the thickness direction. No damage of carbon fiber was observed. Our compression stress result for FAT electrode is much lower than the compression stress of single carbon fiber (3690MPa), mainly due to the tilt of carbon fibers within FAT electrode that caused misalignment and large compression strain.

Thermal measurement

The thermal conductivity measurement system used in this work was consisted of a laser heat source, two calibrated aluminum blocks, a metal block heat sink and an Infrared Camera. The electrode (FAT/slurry-casted thick electrodes) were sandwiched between two Al blocks. A 465 nm blue DPSS (diode-pumped solid-state) laser was applied on the top surface of Al block. The generated heat from the top Al block was conducted to the bottom Al block through the

(FAT/slurry-casted thick electrodes. A FLIR Merlin MID IR camera (320 x 256 pixels) was used to capture and record the temperature during the thermal conductivity measurement.

Electrochemical measurements

The FAT electrodes were assembled in the typical CR2032 coin cells inside an Mbraun MB-200B argon-filled glove box. The Lithium metal was used as the counter and reference electrode. LiPF6 (1.0 M) in a solvent (ethylene carbonate (EC) and diethylene carbonate (DEC), 1: 1 by volume) and Celgard 2500 were used as the liquid electrolyte and separator, respectively. Constant current charge and discharge measurement was carried out Neware Instruments with current density from 0.5mA/cm^2 to 20 mA/cm^2, and its cut-off potential voltage range is 2.15 to 4.2V vs Li/Li+. All measurements were made at 25±0.1 ^{o}C. In the cycle of each test, the battery was first charged and discharged with a small current density of 0.5mA/cm^2. The Electrochemical impedance spectra (EIS) and cyclic voltammogram (CV) were obtained using an electrochemical workstation (BioLogic Science Instruments, VMP3). The measured frequency for EIS is from 0.1 Hz to 100 kHz at room temperature.

Calculation of the porosity of electrodes

X-ray 3D image-reconstruction strategy: The porosity was obtained by calculating the ratio of material occupied area over the total area through X-ray 3D reconstructed cross-section image of the FAT electrodes. The cross-section of the FAT electrode is shown in Figure S6a. We transformed the CT image into a binary grayscale image (Figure S6b), with only two types of voxels representing the area of active material + carbon fibers (black: grayscale intensity: 0) and void area (white: grayscale intensity: 255), respectively. The number of voxels with the 255 gray scale intensity corresponds to the volume of the void space. It allows us to calculate the porosity by simply counting the different types of area/voxels. We assume that the electrode has a uniform

internal structure, and the cross-section of CT image as shown in Figure S6 could represent the real structure of FAT electrode. The porosity of electrode was obtained by the ratio of the area (the number of voxels) of void space and the total area (the total number of voxels) of the FAT electrode. In Figure S6b, the area with the 0 gray scale intensity is 3.68 mm^2 (the number of the voxels is 100080). The area with the 255 gray scale intensity is 2.68 mm^2 (the number of the voxels is 74121) (Table S1). The total area of the FAT electrode in the cross-section is 6.36 mm^2 (the number of the voxels is 174202). Therefore, the calculated porosity is ~42.6%.

Table S1. Parameters obtained from gray image of X-ray 3D reconstructed cross-section computed tomography (CT) image.

	Area (mm2)	Voxels
0 gray scale intensity	3.68	100080
255 gray scale intensity	2.68	74121
Total FAT electrode	6.36	174202

Archimedes method: Archimedes method, also known as fluid saturation method, is based on Archimedes's principle to saturate the pores by a liquid. The electrodes were weighed and immersed into 3.5 ml n-butanol liquid for 2h. And the immersed electrodes were taken out and weighed. The porosity is determined by the equation: Porosity (%) = $(\Delta m/\rho)/v_o \times 100\%$, where Δm is the mass difference of the electrode before and after the adsorption of n-butanol, ρ is the density of n-butanol, and v_o is the total volume of electrode. We assume that the volume occupied by n-butanol equals to the porous volume of the electrode. The density of n-butanol (A-399-4/1-Butanol) is 0.810g/cm^3, the calculated porosity is in Table S2. We tested three samples and the average porosity is 43.8%.

Table S2. The parameters of porosity calculation by Archimedes method.

Parameter	Sample 1	Sample 2	Sample 3	Average value	Error bar
Mass (FAT electrode, mg)	41.16	48.66	32.4	--	--
Mass (FAT electrode + Liquid, mg)	50.87	58.09	40.50	--	--
Volume of electrodes (cm3)	0.0285	0.0247	0.0236	--	--
Porosity (%)	42.1	47.1	42.3	43.8	2.8

Density-composition method: We use the volume ratio of gas in FAT electrode to the total volume of the electrode to calculate the porosity of the electrode. The volume of gas inside the FAT electrode is calculated by subtracting the volume of internal material (LFP, CF and polymer) from the electrode. The tap density of LFP is 1.2 g/cm^3, the density of polymer and carbon black are assumed as 1.0 g/cm^3 and the density of the carbon fibers is 1.78g/cm^3. Hence, the estimation of the porosity of the composite electrodes ($\emptyset$) is:

$$\emptyset = 1 - \frac{V_{internal\ materials}}{V_{total\ FAT\ eletrode}} \quad (1)$$

$$V_{internal\ materials} = \frac{m_{LFP}}{\rho_{LFP}} + \frac{m_{CF}}{\rho_{CF}} + \frac{m_{polymer}}{\rho_{polymer}} \quad (2)$$

$$V_{gas} = V_{total\ FAT\ eletrode} - V_{internal\ materials} \quad (3)$$

The compact density of LFP in the fabricated electrode: The compact density of LFP in FAT electrode is 1.26 g/cm^3. The calculated compact density of LFP in the fabricated FAT electrode is obtained by the ratio of LFP loading (mg) to the volume of electrode (mm^3). We compared the density of our FAT electrode (LFP) with recent reported thick electrodes, and the comparison is shown in Table S3 and Figure S9.

Table S3. Comparison of the compact density of LFP in thick electrode.

Parameter	Loading (Activity materials LFP) (mg/cm^2)	Thickness (mm)	Density (g/cm^3)
Wood-LFP, Hu[1]	60	0.8	0.75
Cellulose-LFP, Hu[2]	20	0.22	0.9
s-CF-LFP, Hu[3]	108	1.35	0.8
Freeze-template-LFP, Huang[4]	85	0.9	0.95
This work	128	1.02	1.26

[1] Chen, C.; Zhang, Y.; Li, Y.; Kuang, Y.; Song, J.; Luo, W.; Wang, Y.; Yao, Y.; Pastel, G.; Xie, J.; Hu, L. Highly Conductive, Lightweight, Low-Tortuosity Carbon Frameworks as Ultrathick 3D Current Collectors. Advanced Energy Materials 2017, 7 (17), 1700595. https://doi.org/10.1002/aenm.201700595.
[2] Kuang, Y.; Chen, C.; Pastel, G.; Li, Y.; Song, J.; Mi, R.; Kong, W.; Liu, B.; Jiang, Y.; Yang, K.; Hu, L. Conductive Cellulose Nanofiber Enabled Thick Electrode for Compact and Flexible Energy Storage Devices. Advanced Energy Materials 2018, 8 (33), 1802398. https://doi.org/10.1002/aenm.201802398.
[3] Li, H.; Peng, L.; Wu, D.; Wu, J.; Zhu, Y.-J.; Hu, X. Ultrahigh-Capacity and Fire-Resistant LiFePO4-Based Composite Cathodes for Advanced Lithium-Ion Batteries. Advanced Energy Materials 2019, 9 (10), 1802930. https://doi.org/10.1002/aenm.201802930.
[4] Huang, C.; Dontigny, M.; Zaghib, K.; S. Grant, P. Low-Tortuosity and Graded Lithium Ion Battery Cathodes by Ice Templating. Journal of Materials Chemistry A 2019, 7 (37), 21421–21431. https://doi.org/10.1039/C9TA07269A.

Table S4. Comparison of the volume capacity with those of existing strategies.

WOOD-LFP (60 mg/cm^2)	Areal current density (mA/cm^2)	0.5	1	2	5	10	Ref[1]
	Areal capacity (mAh/cm^2)	7.5	6.8	5.7	3.8	1.7	
	Volume capacity (mAh/cm^3)	93.75	85	71.25	47.5	21.25	
	Specific capacity (mAh/g)	125	113	95	63	28	
WOOD-LCO (209 mg/cm^2)	Areal current density (mA/cm^2)	0.206	0.412	0.824	2.06	4.12	Ref[2]
	Areal capacity (mAh/cm^2)	24.5	21.9	17.9	16.8	8.2	
	Volume capacity (mAh/cm^3)	240.20	214.71	175.50	164.71	80.50	
	Specific capacity (mAh/g)	118	112	88	76	37.8	
Cellulose-LFP (20 mg/cm^2)	Areal current density (mA/cm^2)	--	1	2	5	10	Ref[3]
	Areal capacity (mAh/cm^2)	--	2.9	2.6	1.8	1	
	Volume capacity (mAh/cm^3)	--	130.63	117.18	81.08	45.05	
	Specific capacity (mAh/g)		145	133	90	50	
rGO/Nb_2O_5 (22 mg/cm^2)	Areal current density (mA/cm^2)	0.4	4.1	9	11.5	13	Ref[4]
	Areal capacity (mAh/cm^2)	3.9	3.8	3.4	2.3	1.45	
	Volume capacity (mAh/cm^3)	--	--	--	--	--	
	Specific capacity (mAh/g)	177	172	154	105	66	
s-CF-LFP (108 mg/cm^2)	Areal current density (mA/cm^2)	0.9	1.8	3.6	5.4	7.2	Ref[5]
	Areal capacity (mAh/cm^2)	16.4	16	15	13	12	
	Volume capacity (mAh/cm^3)	121.48	118.52	111.11	96.29	88.89	
	Specific capacity (mAh/g)	152	139	138	120	111	
Slurry-casted NMC (72 mg/cm^2)	Areal current density (mA/cm^2)	1.116	2.79	5.58	--	--	Ref[6,7]
	Areal capacity (mAh/cm^2)	9.86	9.5	6.2	--	--	
	Volume capacity (mAh/cm^3)	308.3	297	193.5	--	--	
	Specific capacity (mAh/g)	137	132	86	--	--	
3D-printing-LFP (10 mg/cm^2)	Areal current density (mA/cm^2)	0.875	1.75	3.5	7	--	Ref[8]
	Areal capacity (mAh/cm^2)	1.43	1.32	0.76	0.29	--	
	Volume capacity (mAh/cm^3)	35.75	33	19	7.25	--	
	Specific capacity (mAh/g)	143	132	76	29	--	
Freeze-template LFP (85 mg/cm^2)	Areal current density (mA/cm^2)	0.7	1.5	5	10	15	Ref[9]
	Areal capacity (mAh/cm^2)	13.01	12.41	11.73	10.2	7.99	
	Volume capacity (mAh/cm^3)	144.5	137.89	130.33	113.33	88.89	
	Specific capacity (mAh/g)	153	146	138	120	94	
Our work (128 mg/cm^2)	Areal current density (mA/cm^2)	0.5	1	2	5	10	
	Areal capacity (mAh/cm^2)	19.86	19.62	19.20	15.83	7.81	
	Volume capacity (mAh/cm^3)	198.55	196.13	192.01	158.33	78.17	
	Specific capacity (mAh/g)	155	153	150	123	61	

References:

[1] Chen, C.; Zhang, Y.; Li, Y.; Kuang, Y.; Song, J.; Luo, W.; Wang, Y.; Yao, Y.; Pastel, G.; Xie, J.; Hu, L. Highly Conductive, Lightweight, Low-Tortuosity Carbon Frameworks as Ultrathick 3D Current Collectors. Advanced Energy Materials 2017, 7 (17), 1700595. https://doi.org/10.1002/aenm.201700595.

[2] Lu, L.-L.; Lu, Y.-Y.; Xiao, Z.-J.; Zhang, T.-W.; Zhou, F.; Ma, T.; Ni, Y.; Yao, H.-B.; Yu, S.-H.; Cui, Y. Wood-Inspired High-Performance Ultrathick Bulk Battery Electrodes. Advanced Materials 2018, 30 (20), 1706745. https://doi.org/10.1002/adma.201706745.

[3] Kuang, Y.; Chen, C.; Pastel, G.; Li, Y.; Song, J.; Mi, R.; Kong, W.; Liu, B.; Jiang, Y.; Yang, K.; Hu, L. Conductive Cellulose Nanofiber Enabled Thick Electrode for Compact and Flexible Energy Storage Devices. Advanced Energy Materials 2018, 8 (33), 1802398. https://doi.org/10.1002/aenm.201802398.

[4] Sun, H.; Mei, L.; Liang, J.; Zhao, Z.; Lee, C.; Fei, H.; Ding, M.; Lau, J.; Li, M.; Wang, C.; Xu, X.; Hao, G.; Papandrea, B.; Shakir, I.; Dunn, B.; Huang, Y.; Duan, X. Three-Dimensional Holey-Graphene/Niobia Composite Architectures for Ultrahigh-Rate Energy Storage. Science 2017, 356 (6338), 599–604. https://doi.org/10.1126/science.aam5852.
[5] Li, H.; Peng, L.; Wu, D.; Wu, J.; Zhu, Y.-J.; Hu, X. Ultrahigh-Capacity and Fire-Resistant LiFePO4-Based Composite Cathodes for Advanced Lithium-Ion Batteries. Advanced Energy Materials 2019, 9 (10), 1802930. https://doi.org/10.1002/aenm.201802930.
[6] Singh, M.; Kaiser, J.; Hahn, H. Thick Electrodes for High Energy Lithium Ion Batteries. J. Electrochem. Soc. 2015, 162 (7), A1196. https://doi.org/10.1149/2.0401507jes.
[7] Singh, M.; Kaiser, J.; Hahn, H. Effect of Porosity on the Thick Electrodes for High Energy Density Lithium Ion Batteries for Stationary Applications. Batteries 2016, 2 (4), 35. https://doi.org/10.3390/batteries2040035.
[8] Wang, J.; Sun, Q.; Gao, X.; Wang, C.; Li, W.; Holness, F. B.; Zheng, M.; Li, R.; Price, A. D.; Sun, X.; Sham, T.-K.; Sun, X. Toward High Areal Energy and Power Density Electrode for Li-Ion Batteries via Optimized 3D Printing Approach. ACS Appl. Mater. Interfaces 2018, 10 (46), 39794–39801. https://doi.org/10.1021/acsami.8b14797.
[9] Huang, C.; Dontigny, M.; Zaghib, K.; Grant, P. S. Low-Tortuosity and Graded Lithium Ion Battery Cathodes by Ice Templating. J. Mater. Chem. A 2019, 7 (37), 21421–21431. https://doi.org/10.1039/C9TA07269A.

Calculation of the battery components ratios based on the thin electrode stacking configuration and the FAT electrode configuration.

The parameters for conventional slurry thin electrode were obtained from MTI Corporation. The cathode is aluminum foil double side coated by LiFePO4 electrode (170 Ah/kg) (https://www.mtixtl.com/Li-IonBatteryCathode AluminumfoildoublesidecoatedbyLiFePO4241mm.aspx). The single thickness of the electrode is 67.5 μm. The double side active material density is 320 g/m2 (2.37g/cm3). The thickness of the Al foil is 15 μm. The active material proportion of the electrode is 91%.

We assume that the thickness, active material density and active material proportion of anode coating are consistent with that of cathode, and here we are using $Li4Ti_5O_{12}$ as the anode to pair with LFP cathode. The thickness copper foil was 10 μm which was obtained from MTI

Corporation. We used these numbers as baseline of the conventional slurry thin electrode to prepare the Figures 6c-f.

Electrode stacking configuration designs: The conventional slurry thin electrode was stacked by aluminum foil double side coated $LiFePO_4$ cathode, separators and copper foil double side coated by $Li4Ti_5O_{12}$ anode (Figure S13). The thickness of the conventional slurry electrode is 1910 μm. The stacking layers of the Cu foil, Al foil, anode, cathode, and separator were shown in Table S5.

Table S5. Battery components based on the thin electrode stacking configuration and the FAT electrode configuration.

Parameters	Conventional slurry electrode		FAT electrode	
	Layers	Thickness (mm)	Layers	Thickness (mm)
Al foil	6	90	1	15
Cu foil	6	60	1	10
Separators	11	275	1	25
Anode	11	742.5	1	930
Cathode	11	742.5	1	930

The stacking configuration designs of the FAT electrode was shown in Figure 6c. The top-down stacking configuration of FAT battery system model we used is aluminum foil, FAT cathode, separator, FAT anode, and copper foil. In order to further compare the influence of different structural designs (conventional slurry thin electrode and fat electrode) on the battery system, FAT electrode uses the same materials parameters as the conventional electrode to calculate the volume fraction, weight fraction and specific capacity of the FAT battery system. The thickness of the Al foil, Cu foil and the Separator are 15 μm, 10 μm and 25 μm, respectively. The active materials of the FAT cathode and FAT anode are $LiFePO_4$ and $Li4Ti_5O_{12}$, respectively. Because the density of carbon fiber is the same as that of conductive carbon black in conventional slurry thin electrode, we use the same active material density (67.5 μm ≈ 320 g/m^2) as the conventional electrode in

FAT cathode and FAT anode. We used these numbers as baseline of FAT electrode model to prepare the Figures 6c-f. The layers of the FAT electrode model are shown in Table S5.

Calculation of volume fraction: In our conventional and FAT battery system model, all electrodes, Al foil, Cu foil and Separator have area of 1 cm^2 for each. The volume fraction of battery components = h (component thickness) × S (component area)/ V (total volume of the battery system). The calculated volume and volume fraction of the thin electrode stacking configuration and the FAT electrode configuration were shown in Table S6.

Table S6. The volume and volume fraction of the thin electrode stacking configuration and the FAT electrode configuration.

Parameter	Conventional slurry electrode (cm^3)		FAT electrode (cm^3)	
	Volume (cm^3)	Fraction (%)	Volume (cm^3)	Fraction (%)
Anode	0.0742	38.9	0.093	48.7
Cathode	0.0742	38.9	0.093	48.7
Separators	0.0275	14.3	0.0025	1.3
Al foil	0.009	4.7	0.0015	0.8
Cu foil	0.006	3.2	0.001	0.5
Total	0.191	--	0.191	--

Calculation of the weight fraction: The calculated weight fraction of components in battery are shown in Table S7.

Table S7. The weight fraction of the thin electrode stacking configuration and the FAT electrode configuration.

Parameter	Conventional slurry electrode		FAT electrode	
	Weight (g)	Fraction (%)	Weight (g)	Fraction (%)
Anode	0.1933	39.4	0.2422	48.5
Cathode	0.1933	39.4	0.2422	48.5
Separators	0.0250	5.2	0.0023	0.5
Al foil	0.0243	5.0	0.0040	0.8
Cu foil	0.0538	11.0	0.0090	1.7
Total	0.4898	--	0.4997	--

Calculation of the capacity: We use electrode specific capacity of 170 mA/g to calculate the gravimetric and volumetric capacity of batteries. Based on the volume and weight calculation in previous tables, the gravimetric capacity for conventional stacking electrode-based battery and FAT electrode-based battery are 61.1 Ah/kg, and 82.5 Ah/kg, respectively. And the volumetric capacity for conventional stacking electrode-based battery and FAT electrode-based battery are 156.6 Ah/L and 213.3 Ah/L, respectively.

Calculation of the energy: We use 2.0 V as the working voltage for LFP/LTO cell. The gravimetric energy density for conventional stacking electrode-based battery and FAT electrode-based battery are 122.1 Wh/kg, and 164.8 Wh/kg, respectively. And the volumetric energy density for conventional stacking electrode-based battery and FAT electrode-based battery are 313.3 Wh/L and 431.2 Wh/L, respectively.

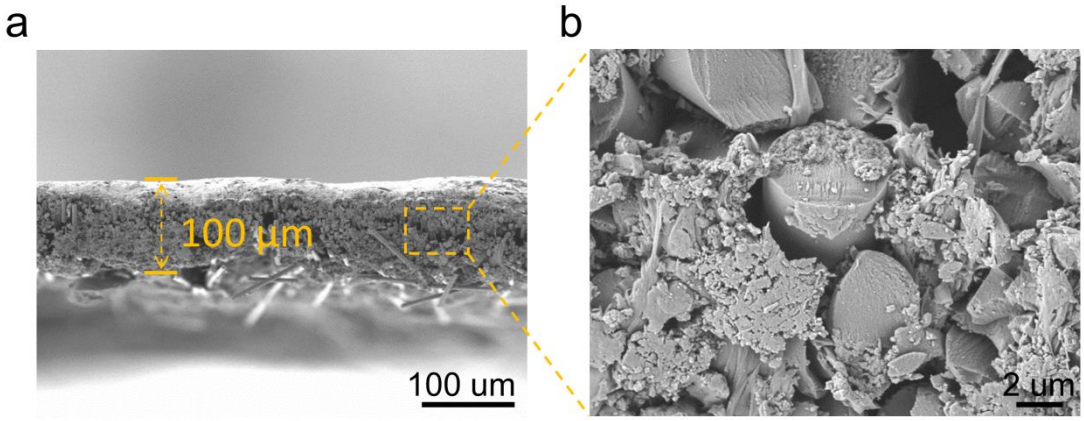

Figure S1. The images for the prepared composite ultra-thin FAT electrode film structure. The carbon fibers are uniformly distributed in the LFP nanoparticles and tightly wrapped by the LFP particles.

Figure S2. A large FAT electrode with diameter of 18 mm and height of ~55 mm for potential 18650 cylindrical cell application.

Figure S3. Photo image of slurry-cased electrode. After drying, cracks occurred in the thick electrode.

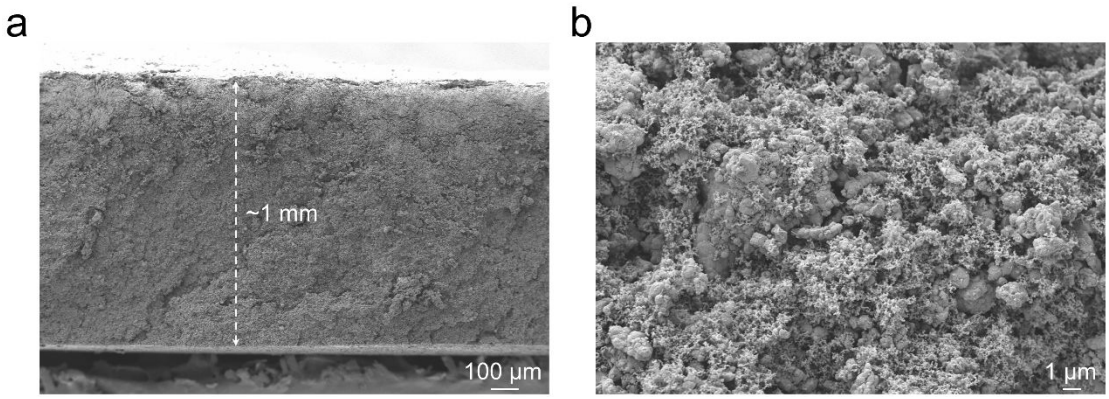

Figure S4. (a) The SEM images and (b) magnified SEM images of the slurry slurry-cased electrode.

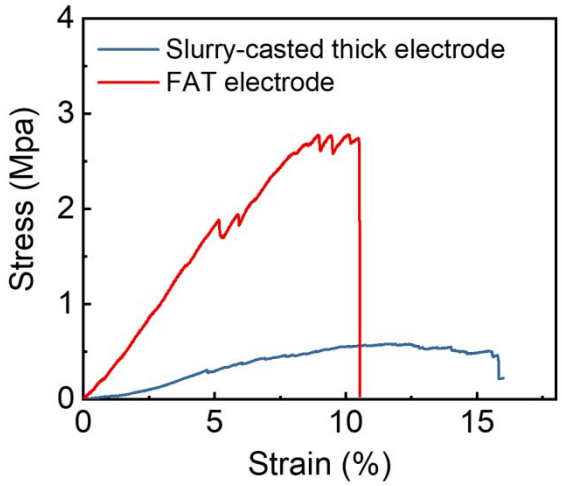

Figure S5. Compression stress-strain curves of fiber-aligned thick electrode and slurry-casted thick electrode.

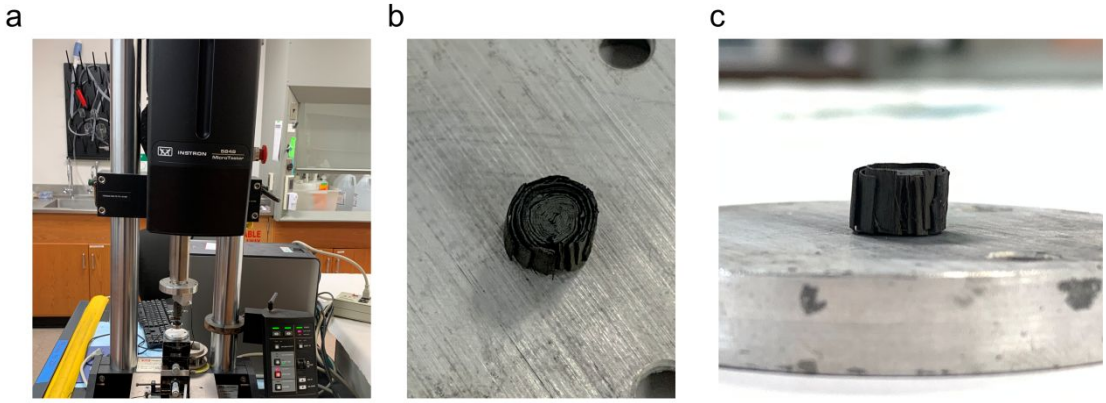

Figure S6. (a) Instron compression testing setup. (b) Top view of FAT electrode after compression. (c) Side view of FAT electrode after compression.

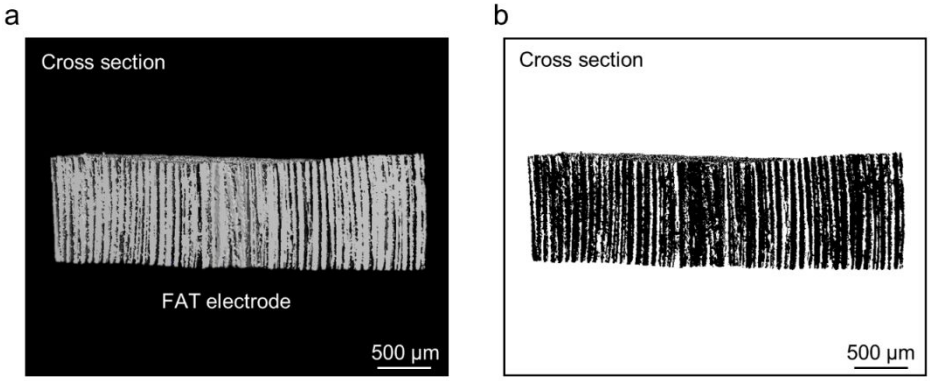

Figure S7. (a) X-ray 3D reconstructed cross-section computed tomography (CT) image of FAT electrode. (b) Gray image obtained by transforming the same CT image into a binary grayscale image with only black and white color to represent the materials and void space, respectively.

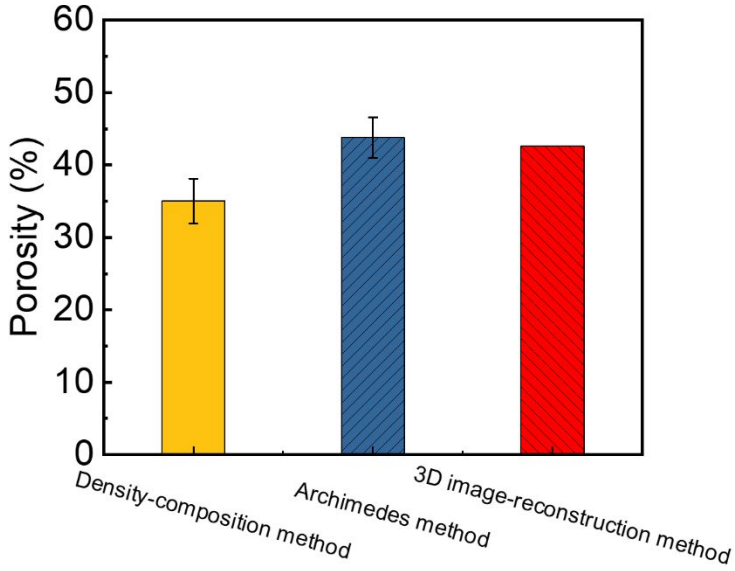

Figure S8. Comparison of porosity obtained by three methods: density-composition method, Archimedes method, and 3D image-reconstruction method.

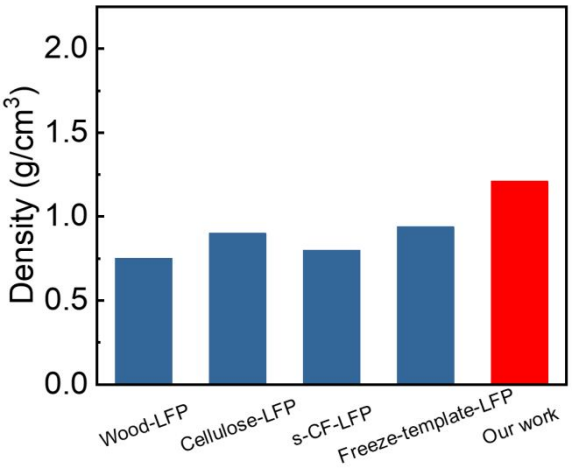

Figure S9. Comparison of density of LFP in thick electrode.

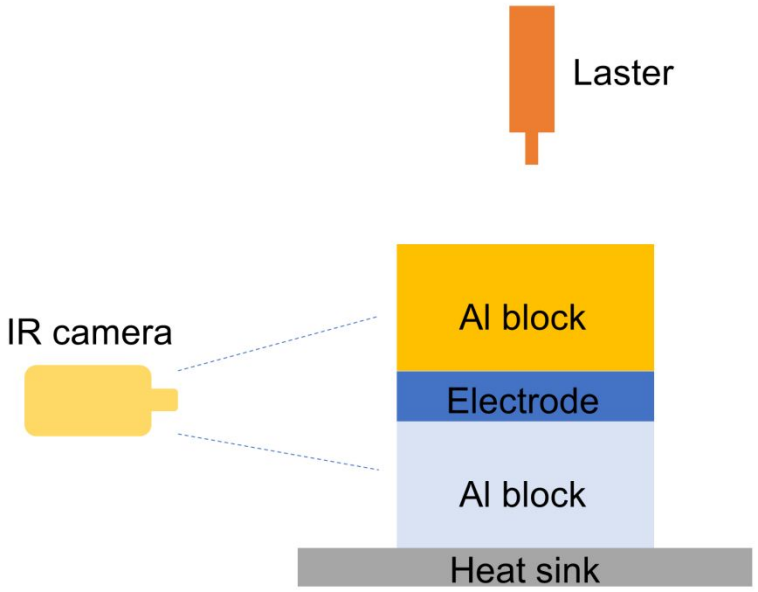

Figure S10. Schematic of laser-IR camera thermal conductivity test system.

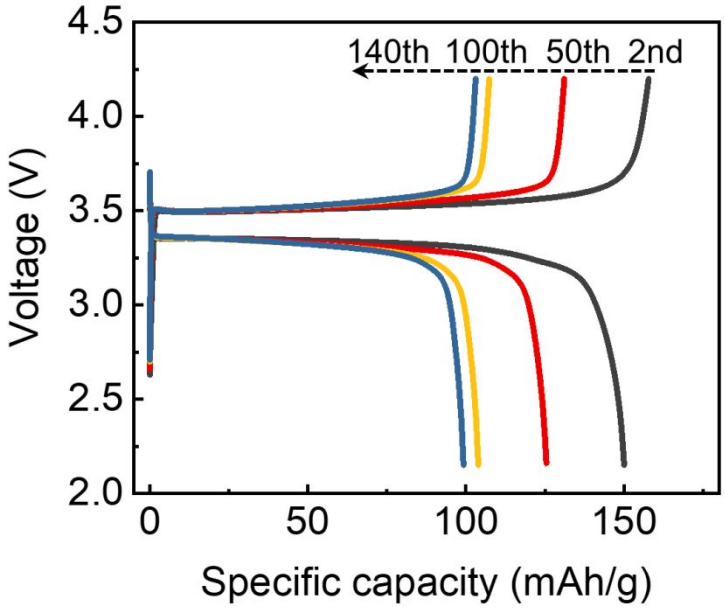

Figure S11. The cyclic charge-discharge curves of the FAT electrode at 2nd, 50th, 100th and 140th under 2 mA/cm^2.

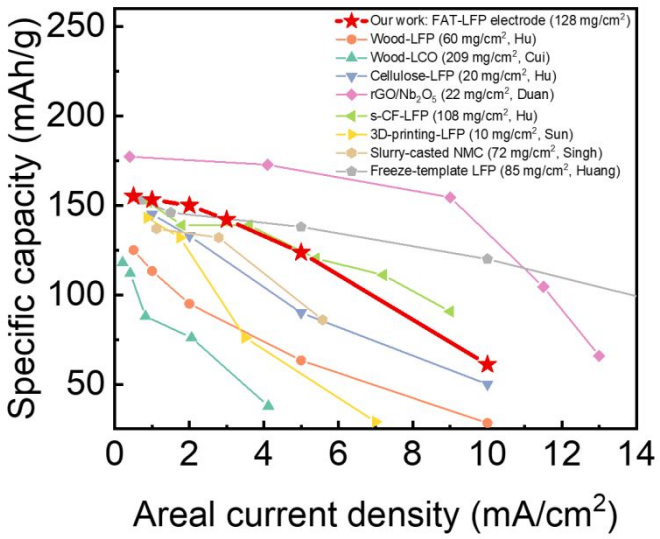

Figure S12. Comparison of the FAT electrode and previously reported thick electrodes in the aspect of specific capacity.

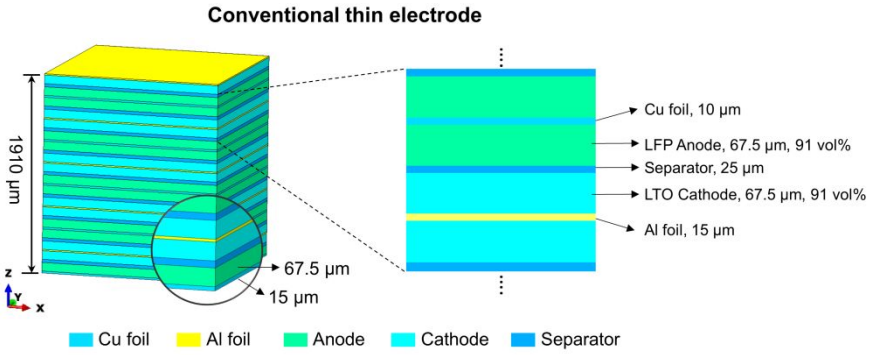

Figure S13. Electrode stacking configuration designs of conventional electrode.